INTERPRETING RECENT OBSERVATIONS OF He I 10830 Å

HARRISON P. JONES

NASA/Goddard Space Flight Center, Laboratory for Astronomy and Solar Physics, Greenbelt, MD 20771, U.S.A.

Abstract. Spectra-spectroheliograms obtained in the 10830 Å line with the NASA/NSO Spectromagnetograph are analyzed to produce images in equivalent width, line depth, velocity, and continuum intensity. These and other images imply that if large-scale deficits in coronal irradiation induce weakening of the 10830 line, the ionizing radiation must be produced in close enough spatial proximity to the region of formation for 10830 to allow sharply defined spatial boundaries. The complex morphology of the images shows the importance of underlying chromospheric structure in providing a highly variable "substrate" which is modulated by varying illumination. Clear evidence is seen of He I 10830 Å formation in magnetic loops where the velocity field, particularly at footpoints, directly affects the excitation of the line. Steady flows as seen by Lites *et al.* (1985) are also observed, particularly near the limb. The observations and radiative transfer calculations are consistent with a simple, optically thin "cloud" model of line formation, and observed line profiles in weak network elements compare favorably with predictions from mean models.

Key words: He I 10830 Å – infrared: stars – line: formation – Sun: atmosphere – techniques: spectroscopic

1. Introduction

The 10830 Å line of He I is seen in emission just above the solar limb and in weak absorption on the disk with strong spatial and temporal variations. Since the atomic transition occurs between the lowest metastable levels of orthohelium which are both energetically far above ($\sim$ 20 eV) and radiatively isolated from the true ground state (parahelium), excitation of the line occurs primarily as recombination from He II. The precise mechanisms responsible for the formation of the He I 10830 Å line are still a matter for considerable speculation and controversy. However, the rich phenomenology evident in 10830 Å images and the well-documented correlations of many 10830 Å features with EUV and soft X-ray phenomena are ample evidence of the importance of the line in solar physics.

Radiative transfer calculations with mean models (Avrett, 1991; Avrett *et al.*, 1993) place the formation of the line near the interface between the upper chromosphere and the lower transition region and show the sensitivity of the lower-level population to ionizing radiation produced in the surrounding transition region and corona and to chromospheric density. These calculations are consistent with the observed limb emission, the well established visibility of coronal holes in 10830 Å spectroheliograms, the high correspondence between 10830 Å spectroheliograms and soft X-ray images of the Sun, and the good temporal correlations between integrated 10830 Å "fluxes" and other proxies for EUV irradiance (Harvey, 1984, 1993).

In this paper, some early 10830 Å observations from a new instrument, the NASA/NSO Spectromagnetograph (SPMG: Jones *et al.*, 1992), are described which may help to quantify the mechanisms for He line formation and their observational consequences. The SPMG is now in routine operation at the NSO/Kitt Peak Vacuum Telescope (KPVT) and will soon replace the aging 512-channel Diode Array Magnetograph (Livingston *et al.*, 1976 a,b). Instead of the two-slit Babcock configuration of the old instrument, the SPMG images resolved, two-dimensional, long-

D. M. Rabin et al. (eds.), Infrared Solar Physics, 49–58.

https://doi.org/10.1017/S0074180900124246 Published online by Cambridge University Press

slit spectra over a several-Ångstrom bandpass on a CCD detector. Special video processing electronics accumulate and record or reduce the resolved line profiles synchronously with spatial scanning of the solar image across the entrance slit of a spectrograph. Thus the many monochromatic images and quantities derived from them are strictly simultaneous and precisely registered. Fortunately, the detector (Texas Instruments 241 chip) responds well enough at 1.083 μm without special cooling to produce far fewer "streaks" from slow "fixed" pattern variations than the Diode Arrays of the old instrument.

2. Observations

The observations described here were taken in conjunction with a rocket flight of the NASA/Goddard Solar Extreme Ultraviolet Rocket Telescope and Spectrograph (SERTS)-4 (Neupert *et al.*, 1992) on May 7, 1991. Figure 1 shows a full-disk magnetogram and 10830 Å spectroheliogram taken with the SPMG at the KPVT prior to the rocket flight. Comparison of the SPMG 10830 Å and magnetic data with EUV spectra and images obtained by the SERTS instrument is in progress and will be reported separately as appropriate. This paper treats the SPMG data alone.

Various solar features seen in 10830 Å are labeled for reference in Figure 1. When seen in negative contrast, coronal holes appear as slightly brighter (lower absorption) regions in 10830 Å equivalent width images which overly unipolar magnetic fields; three large coronal holes, labeled CH_{1-3} are marked in Figure 1. A similar region of slightly enhanced brightness which is labeled FC overlies a region of weak magnetic field between two unipolar regions of opposite polarity and is probably a "filament channel" (McCabe and Mickey, 1981). Outside of coronal holes and filament channels, the magnetic field patterns can be seen as network-like, weak absorption features in the 10830 Å image. Concentrated dark points which tend to be associated with X-Ray bright points (Harvey, 1985) can be seen at various points as can dark filament- and loop-like structures. As discussed below, the small bright features in the large southwest active region are artifacts of high line-of-sight motions.

Even though coronal holes as seen in Figure 1 and other He 10830 Å data are low contrast phenomena, they are consistently outlined by sharp, if irregular, boundaries. Lites *et al.* (1985) point out that if the He 10830 Å contrast in coronal holes is a result of reduced excitation by EUV and soft-Xray radiation incident from above, this radiation must originate close to the He I line-forming region. Otherwise the spatial signature would be more diffuse. However, the boundaries often appear as well-formed network and could indicate a density enhancement surrounding the base of the coronal hole. Either explanation argues for thermodynamic manifestations of coronal holes to be at least as deeply rooted as the chromosphere/transition-region boundary.

The full-disk images were followed by ten He 10830 Å equivalent width area scans of the target region for the SERTS-4 instrument at one image every 15 minutes. Although no dramatic event was recorded in these area scans and they are not shown here, rapid viewing of the images in sequence leaves an impression of a very "busy" field of view with many rapid but small-scale changes occurring. This

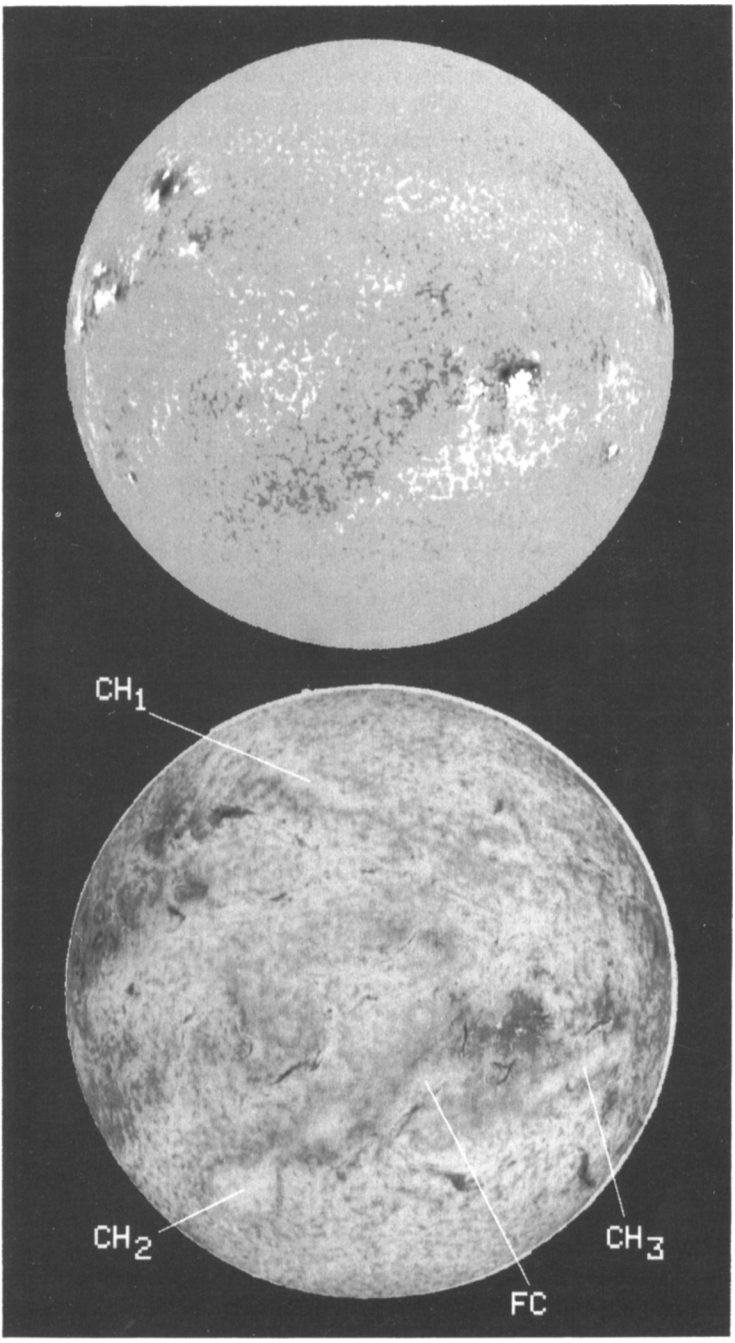

Fig. 1. Upper: full-disk magnetogram (Fe I, 8688 Å), 7 May 1991, 15:36-16:26 UT. Lower: full-disk 10830 Å equivalent width spectroheliogram, 16:40-17:22 UT, shown with negative contrast; labeled features are described in text

https://doi.org/10.1017/S0074180900124246 Published online by Cambridge University Press

is particularly evident in some of the dark filamentary structures where absorption features appear to move back and forth along lines of force.

Figure 2 shows continuum intensity (top), line-of-sight velocity, a sample spectral section along a row marked by horizontal fiducials on each image, equivalent width, and line-center depth (bottom) derived from the He 10830 Å spectra-spectroheliogram. The labeled vertical lines point to the positions of selected features along the spectral section whose line profiles are shown in Figure 3.

The continuum image shows contamination from the weakest member of the 10830 Å triplet (10829.1 Å). The velocities are quite large compared to photospheric values with the grey scale covering the range from -8 to +7 km s^{-1}. Both line depth and equivalent width are shown here in negative contrast (small values appear brighter) as in the conventional display of NSO/KP 10830 Å spectroheliograms. Notice the nearly identical appearance of the line depth and equivalent width– a correlation which is easily explained if the lines are optically thin as discussed below. The morphology in and near the active region is complicated and clearly suggestive of line formation in magnetic loops and filaments. The regions of highest velocity tend to coincide with the apparent footpoints of these magnetic features at locations which are often marked by increased absorption or apparent emission (see below).

The contrast of the spectrum is enhanced by a non-linear grey-scale mapping; the line is quite weak (typically with depths of just a few percent of the continuum) at most places in the image. All of the images (not the spectra) have had center-to-limb trends and residual streaks from imperfect fixed pattern correction removed by simple curve fitting techniques. The labeled fiducials point to: A) a background or "quiet sun" feature; B) a network feature; C) a short active-region filament or loop; D) an artificial "emission" feature (see below); and E) a long-lived, network-like velocity structure as seen, for example by Lites *et al.* (1985) near the limb.

3. Interpretation

Line profiles for the five labeled features of Figure 2 are shown in Figure 3. The horizontal bars above the graph delimit two different wavelength bands which were used during the course of this analysis to determine the continuum intensity. The profiles of Figure 3 and the images of Figure 2 were derived using the two lower continuum bands. An immediate difficulty can be seen to arise in high-velocity features such as "D" where the line has been shifted partially into one of the continuum bands; the artificially induced reduction in continuum intensity forces part of the line into apparent emission and reduces both the line depth and equivalent width. The upper single band was used for an initial analysis of the data and is similar to the "two-slit" algorithm used for the synoptic full-disk spectroheliogram. In this case, the effect is enough to produce a negative (emission line) equivalent width. The difference in equivalent width images with the different determinations of continuum is shown in Figure 4. The single-band determination shows several artificial emission features and a number of small, low contrast "speckles" which are wholly absent in the image with the two-band determination of continuum. For future data taken with the SPMG, the continuum will be selected from spectral

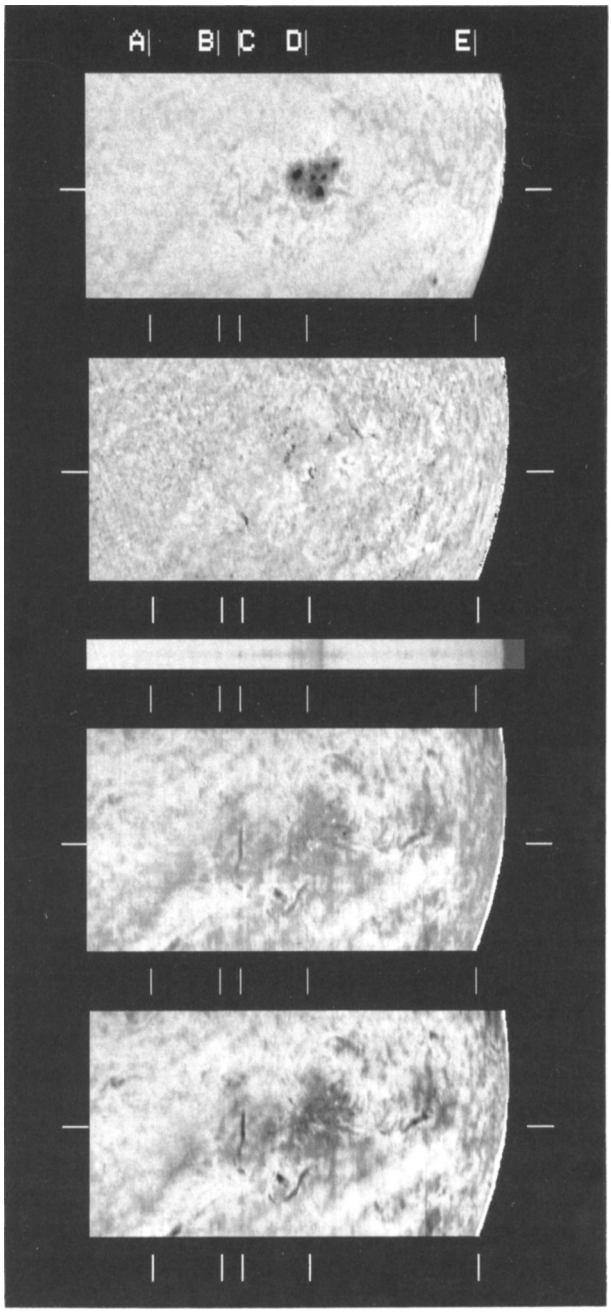

Fig. 2. Continuum intensity (*top*), velocity, spectral section (λ increasing from bottom to top), equivalent width, and line depth (*bottom*) images derived from a He 10830 Å spectra-spectroheliogram. The image row for the spectrum and specific labeled features are marked at the borders (see text).

https://doi.org/10.1017/S0074180900124246 Published online by Cambridge University Press

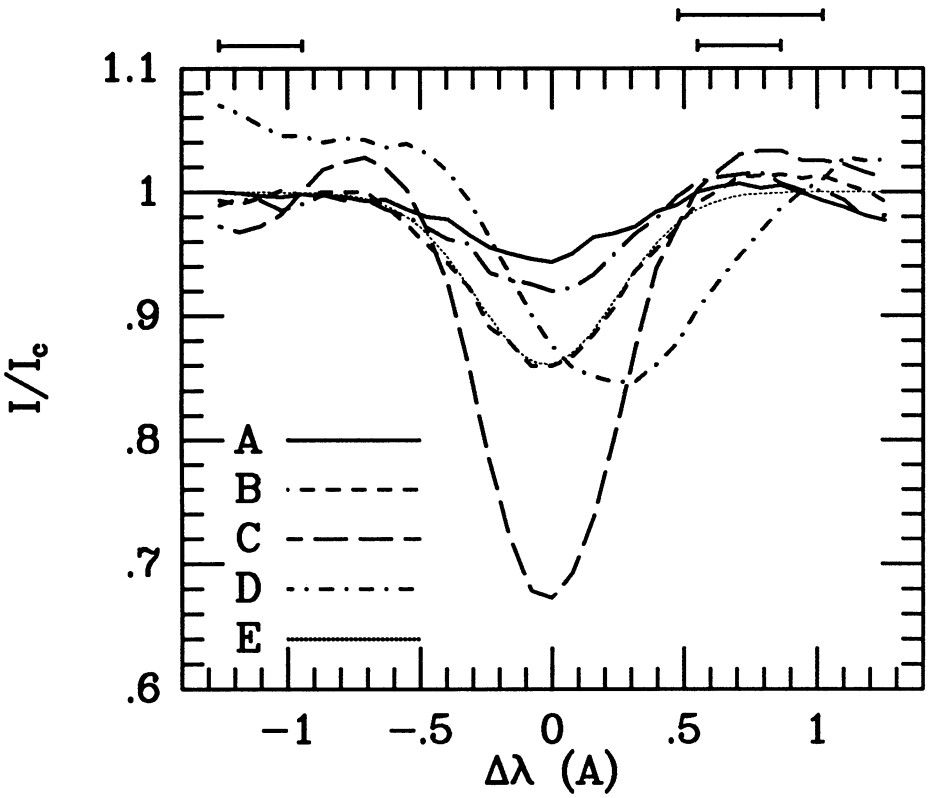

Fig. 3. Line profiles for features labeled in Figure 2. The light dotted line near the profile for feature "B" is a fit as described in the text. Horizontal bars above the graph delimit two different continuum bands used for analysis

region which is far enough removed to be unaffected by Doppler shifts.

There is a weak water vapor line almost exactly coincident with the 10830 Å line (Breckenridge and Hall, 1973; see also Harvey, 1993) whose effective Doppler width is typically 60 mÅ (much smaller than that for the He line) and which can increase the central depth by the order of 1% of the continuum (a noticeable effect where the line is weak). No account of water vapor has been taken here, but the qualitative results are not seriously affected.

While no attempt is made in this paper to produce detailed self-consistent non-LTE models based on the data, some approximate quantitative constraints can be determined by noting that both the observations and average models are consistent with a "cloud" model of line formation (Grossman-Doerth and von Uexküll 1971, 1973); that is, along any line of sight the region of appreciable He I 10830 Å absorption and emission is confined to a narrow spatial domain well above and separated

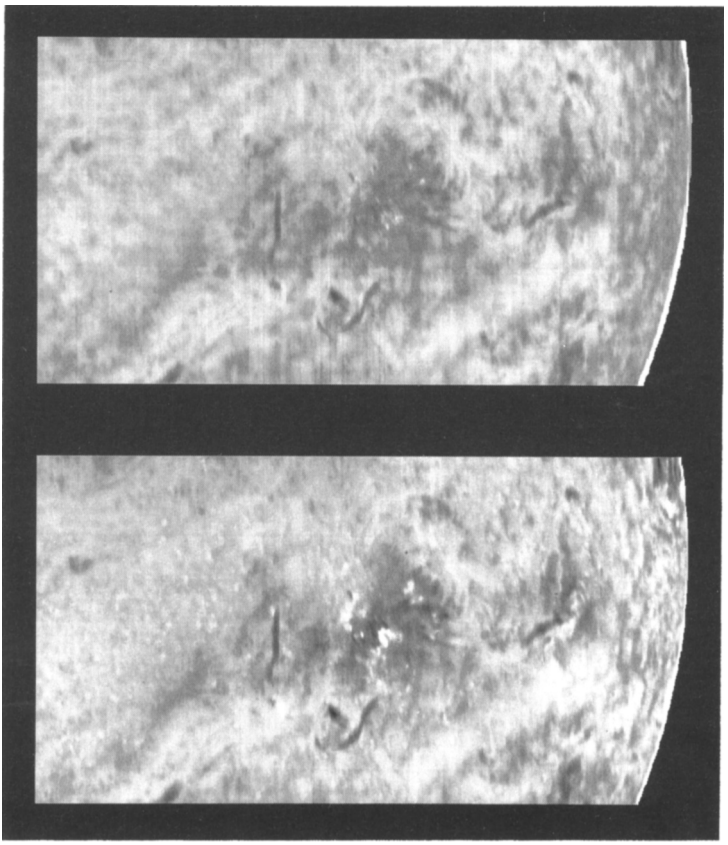

Fig. 4. Equivalent width images calculated using two continuum bands (top) and a single continuum band (bottom) as shown in Figure 3.

from the photosphere which produces the background continuum. If the line source function is approximately constant and independent of wave length in this cloud of line-forming material, then the equation of transfer has the particularly simple solution

$$I(\lambda) \approx I_c \exp(-\tau(\lambda) + S(1 - \exp(-\tau(\lambda)). \quad (1)$$

In terms of line-depth, $d(\lambda) \equiv 1 - I(\lambda)/I_c$, equation (1) leads simply to

$$d(\lambda) = (1 - S/I_c)(1 - \exp(-\tau(\lambda)) \rightarrow (1 - S/I_c)\tau(\lambda), \quad (2)$$

where the limit ($\tau(\lambda) \ll 1$) is valid for optically thin clouds.

The solar absorption feature at 10830 Å is actually the blend of two members of the $2\ ^3S$–$2\ ^3P$ triplet separated by $\delta = 0.091$ Å with the statistical weights of the longer to the shorter wave-length lines having the ratio $r = 5/3$. Thus, if τ_0 denotes

https://doi.org/10.1017/S0074180900124246 Published online by Cambridge University Press

the sum of all the line-center optical depths of each of the Zeeman sub-states for the two lines, we may write

$$\tau(\lambda) = [(1-\alpha)\phi(\lambda-\lambda_1) + \alpha\phi(\lambda-\lambda_1+\delta)]\tau_0 \quad (3)$$

where λ_1 is the line center wavelength of the longer-wavelength line, $\alpha = r/(1+r)$, and the profile coefficient ϕ is expressed in terms of Doppler width λ_D as approximately

$$\phi(\lambda) = \exp(-(\lambda/\lambda_D)^2). \quad (4)$$

Anticipating the observed fact that $\delta/\lambda_D < 1$, one finds that τ and, hence, d have a maximum at wavelength

$$\lambda^* = \lambda_1 - \alpha\delta \quad (5)$$

from which it follows that the equivalent width, $w = \int_0^\infty d(\lambda)d\lambda$, is related to maximal line depth $d^* = d(\lambda^*)$ by

$$w/d^* = \sqrt{\pi}\lambda_D/[1-\alpha(1-\alpha)(\delta/\lambda_D)^2]. \quad (6)$$

Finally, one may use equation (6) to find the Doppler width from the observed equivalent width and maximum line depth. One Newton-Raphson iteration with an initial guess of $\lambda_D^\circ = w/(\sqrt{\pi}d^*)$ of the cubic equation for λ_D which results from equation (6) yields

$$\lambda_D \approx \frac{w}{\sqrt{\pi}d^*}[1 - \pi\alpha(1-\alpha)\delta^2/(w/d^*)^2]. \quad (7)$$

The light dotted line which nearly coincides with the profile for feature "B" in Figure 3 is the calculated "fit" of the sum of two Gaussians, appropriately weighted and shifted according the multiplet structure for the 10830 Å line, with a Doppler width as determined by equation (7); clearly the approximations made in the preceding development lead to consistent representations of the data.

Table I shows the equivalent widths, line depths, and Doppler widths calculated from equation (7) for each of the labeled features of Figures 2 and 3 together with the same parameters derived graphically from the model calculations of Avrett (1991). The Doppler width from equation (7) is shown in Å, as a velocity (km s^{-1}), and as the temperature (K) required to produce the observed width from purely thermal motions. An obvious feature of the observed profiles is that they are much too broad to be explained by purely thermal motions if the models are even approximately correct. The wavelength profile coefficient for optical depth as computed from the height variations of temperature and lower level population shown by Avrett (1991) without macroturbulence or microturbulence, for example, shows an effective Doppler width corresponding to a temperature of about 8300 K. Thus substantial spatially unresolved velocities, with amplitudes approximating the range of resolved velocities, are required to explain the width of the line.

One should not take comparisons between the model and observed results too seriously, since the models were not constructed to explain these data. Although the model profiles look qualitatively very much like observed ones, the observed

TABLE I
Line Profile Parameters

Feature	w(Å)	d^*	λ_D Å	λ_D km s^{-1}	K
		Observations			
A: Quiet Sun	0.045	0.055	0.456	12.6	38700
B: Network	0.095	0.141	0.373	10.3	25900
C: AR Filament	0.174	0.328	0.292	8.1	15800
D: High-Velocity	0.069	0.152	0.250	6.9	11600
E: Limb Network	0.060	0.078	0.430	11.9	34300
		Models (Avrett, 1991)			
Cell Interior:	0.008	0.022	0.210	5.8	8200
Average Sun:	0.020	0.033	0.345	9.6	22100
Bright Network:	0.035	0.060	0.328	9.1	20000
Plage:	0.048	0.090	0.300	8.3	16700

profiles tend to be both deeper and broader than the calculated ones, suggesting that the observed features have higher density and more extreme "turbulence" than the models. The recent calculations of Avrett *et al.* (1993), however, show larger central line depths and correspond better with the observations. Also, the models clearly do not (nor were they intended to) represent the darkest features of the observations such as the numerous filaments and loops. These features are perhaps more aptly approached by radiative transfer methods which have been applied to prominences (Heasley *et al.*, 1974; Heasley and Milkey, 1976, 1978).

The shapes of the profiles are all consistent with optically thin, Gaussian lines, and it is not possible to infer both the line source function and the optical depth from the observed profile which, from equation (2), depends only on the product. However, some limits can be established because He I 10830 Å features appear darker than the underlying continuum so that $0 < S < I_c$. Thus, line-center optical depths do not exceed a few tenths [$S = 0$ in Eq. (2)]. Moreover, if the temperature regime of the models is even roughly correct, the line is underexcited since the source function must be less than the Planck function of about 5000 K typical of the photosphere ($S = I_c$ in equation (2)), but the line-forming plasma has typical high-chromospheric electron temperatures in excess of 8000 K.

https://doi.org/10.1017/S0074180900124246 Published online by Cambridge University Press

4. Conclusions

The observations presented here lend support to a dual mechanism for formation of He I where coronal radiation enchances recombination of He II in a highly structured chromosphere. Large velocities of He-forming material can drastically alter the appearance of equivalent-width or line-depth images if the continuum is taken too close to the nominal line center. Thus, in spite of apparent emission in NSO/KP synoptic data, the He I 10830 Å line is always seen in absorption on the disk except possibly in flares. The line appears to be optically thin everywhere on the disk, and unresolved velocity fields approaching 10 km s^{-1} are needed to explain the observed line widths. The observed profiles appear typically to be both broader and deeper than those calculated by Avrett (1991). More detailed modeling and comparison of this and other data with nearly simultaneous and co-spatial EUV and soft X-ray data is planned or in progress and should lead to a more quantitative understanding of some of the phenomena described here.

Acknowledgements

The author is pleased to acknowledge many useful conversations with J. Harvey, K. Harvey, and E. Avrett in preparing this presentation, and T. Duvall for his assistance with the observations. NSO/Kitt Peak data used here are produced cooperatively by NSF/NOAO, NASA/GSFC, and NOAA/SEL, and the research is partially funded by Supporting Research and Technology grants from the Space Physics Division of the NASA Office of Space Science and Applications.

References

Avrett, E. H.: 1991, in *Workshop on the Solar Electromagnetic Radiation Study for Solar Cycle 22*, R. F. Donnelly, ed., NOAA ERL, Boulder.
Avrett, E. H., Fontenla, J. M., and Loeser, R.: 1993, these proceedings.
Breckenridge, J. B. and Hall, D. N. B.: 1973, *Solar Phys.* **28**, 15.
Grossman-Doerth, U. and von Uexküll, M.: 1971, *Solar Phys.* **20**, 31.
Grossman-Doerth, U. and von Uexküll, M.: 1971, *Solar Phys.* **28**, 333.
Harvey, J.W.: 1984, in *Solar Irradiance Variations on Active Region Time Scales*, B.J. LaBonte *et al.* eds., NASA CP-**2310**, 197.
Harvey, J. W.: 1993, these proceedings.
Harvey, K. L.: 1985, *Aust. J. Phys.* **38**, 875.
Heasley, J. N., Mihalas, D., and Poland, A. I.: 1974, *Astrophys. J.* **192**, 181.
Heasley, J. N. and Milkey, R. W.: 1976, *Astrophys. J.* **210**, 827.
Heasley, J. N. and Milkey, R. W.: 1978, *Astrophys. J.* **221**, 677.
Jones, H. P., Duvall, T. L. Jr., Harvey, J. W., Mahaffey, C. T., Schwitters, J. E., and Simmons, J. E.: 1992, *Solar Phys.* **139**, 211.
Lites, B. W., Keil, S. L., Scharmer, G. B., and Wyller, A. A.: 1985, *Solar Phys.* **97**, 35.
Livingston, W. C., Harvey, J., Pierce, A. K., Schrage, D., Gillespie, B., Simmons, J., and Slaughter, C.: 1976a, *Appl. Optics* **15**, 33.
Livingston, W. C., Harvey, J., Slaughter, C., and Trumbo, D.: 1976b, *Appl. Optics* **15**, 40.
McCabe, M. K. and Mickey, D. L.: 1981, *Solar Phys.* **73**, 59.
Neupert, W. N., Epstein, G. L. and Thomas, R. J.: 1992, *Solar Phys.* **137**, 87.